# Performance Tests of Two Precision Attitude Determination Systems

K.J. McAloon,* R.L. Farrenkopf,† F.J. Belsky,‡ and R.J. Mann§
*TRW Defense and Space Systems Group, Redondo Beach, Calif.*

**Results of laboratory performance tests of two satellite attitude determination systems are given. One system employed a strapdown star tracker and gyro assembly, the other a single-axis, gimbaled star tracker and a gyro assembly. The laboratory tests simulated those orbit conditions that would be experienced on a three-axis stabilized, earth pointed satellite in geosynchronous orbit. A ground-fixed laboratory test was performed in which system axes remained stationary in the laboratory coordinates while revolving star beams stimulated the star trackers. The laboratory instrumentation techniques used to meet the stringent accuracy requirements are described. Results are presented which show both systems met the performance goal of 3.6 arc-s. Comparative analyses of both systems are also discussed.**

## I. Introduction

THE need for precision attitude determination systems (PADS) on board satellites has been well established by the requirements of astronomical and earth-pointing payloads over the last decade. With growing frequency PADS accuracy requirements are extending to the arc-second level. Based on early design and analysis efforts,[1,2] two such PADS have been developed within the last few years: one employing a strapdown star tracker,[3] and gyros, the other using a single-axis, gimbaled star tracker and gyros. The gimbaled tracker design was based on an earlier two-axis version.[4] Both systems were designed for an accuracy of 3.6 arc-s ($1\sigma$) per axis.

The objective of the effort described in this paper was a laboratory evaluation of both PADS at the system level. Previous efforts[5-7] to demonstrate this accuracy had shown the difficulties introduced by laboratory instrumentation errors. However, a test simulating a geosynchronous orbit application presents an opportunity to minimize such errors, permitting test results to be recorded as measured, rather than being modified for instrumentation errors. The primary focus of this effort was on the error contribution of the star trackers, and the effectiveness of the software algorithms in functioning with actual sensor signals.

## II. PADS Description

A satellite attitude determination system provides a measurement of the inertial attitude of its reference axes. The attitude of the spacecraft or payload axes is determined through a known transformation to the PADS reference axes. A functional block diagram of PADS is shown in Fig. 1. The sensors consist of 1) a star tracker that provides periodic updates of attitude relative to identified stars, and 2) gyros that provide a continuous indication of the relative inertial attitude. The sensor signals are processed in a digital computer (either on board or ground based). The computer software algorithms combine the redundant sensor signals and compute the inertial attitude of the PADS reference axes.

In orbit, a strapdown star tracker uses the orbit rate of the satellite for star availability. A gimbal star tracker has the added capability of scanning a portion of the celestial sphere to acquire stars.

Both PADS used in the laboratory evaluation were designed to operate in geosynchronous orbit with an accuracy better than 3.6 arc-s ($1\sigma$) per axis.

### Hardware

The PADS hardware which was tested in the laboratory is also illustrated in Fig. 1. Two PADS configurations were evaluated, one using the strapdown star tracker, the other a single-axis, gimbaled star tracker. The same three-axis, inertial reference unit was used for each configuration. This unit contained three single-degree-of-freedom gyros. Assuming PADS uses a ground-based computer, the sensor data were collected on magnetic tape during the test using a small laboratory computer, and then processed post-test using a larger general-purpose computer.

The strapdown star tracker is a high-accuracy, high-sensitivity sensor with the characteristics listed in Table 1. The small $1\times1$ deg field of view results from the accuracy requirement of 2.0 arc-s from the star line of sight to the sensor electro-optical axes. A star magnitude sensitivity of 8 $M_v$ is required to provide frequent star updates in the field of view at geosynchronous rate. The tracker used in the test evaluation has a sensitivity of 10 $M_v$.

An image dissector tube is used in the strapdown star tracker. The tracker operates in the photon-counting mode with all digital electronics to provide the 10 $M_v$ sensitivity. Graphite/epoxy composite material is used in the mechanical structure for thermal stability.

The gimbaled star tracker consists of a star sensor unit mounted within a single-degree-of-freedom gimbal assembly. Its design characteristics are listed in Table 2. The $0.5\times0.5$ deg instantaneous field of view can be gimbaled through a 90-deg arc. As a consequence, a star magnitude sensitivity of only 3.5 $M_v$ is required to provide star update periods comparable to those of the strapdown star tracker in geosynchronous orbit.

The star sensor unit also uses an image dissector tube, operated in the conventional analog mode because of the reduced sensitivity requirement. The gimbal assembly utilizes a single ball/flexure suspension system and an inductosyn readout.

The inertial reference unit is the engineering model developed for the Orbiting Astronomical Observatory. Its three gyros are mounted with their input axes orthogonal to each other. Floated, single-degree-of-freedom gyros are used. They are operated with binary, pulse-restrained torque loops.

Presented as Paper 77-1039 at the AIAA 1977 Guidance and Control Conference, Hollywood, Fla., Aug. 8-10, 1977; submitted Oct. 26, 1977; revision received Jan. 19, 1978. 

Index category: Spacecraft Technology; Spacecraft Systems.

*Senior Staff.
†Senior Staff. Member AIAA.
‡Member of Technical Staff. Member AIAA.
§Member of Technical Staff.

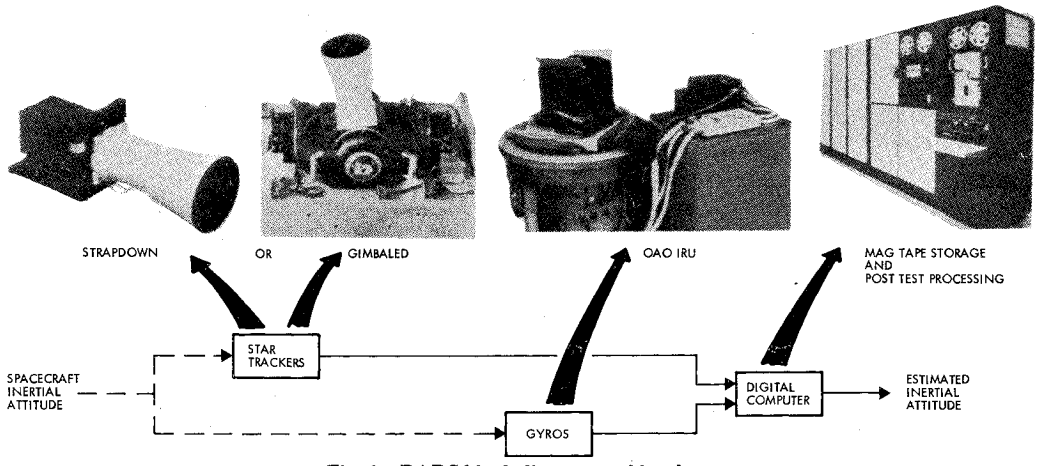


**Fig. 1 PADS block diagram and hardware.**

Characteristics of the unit are presented in Fig. 2. Random-drift performance is characterized by plots of the standard deviation of gyro attitude output as a function of sample time. The standard deviation after 20 min for the $x$ and $y$ gyros is approximately 1 arc-s. The deviation for the $z$ gyro is 4 arc-s after 20 min. The zero slope of the short-term performance is due to pulse quantization. All data were taken with the gyros mounted on an isolated seismic pad.

It is noted that the long-term performance indicated in Fig. 2 is not typical for this class of gyro.[8] Individual analysis of the drift rate time plots indicated that the slope of plus one shown in the $x$ and $y$ gyro plots was due to a periodic change in drift rate, probably due to a thermal sensitivity. The $z$ gyro performance was somewhat poorer and was variable from day to day. This variability is evidenced by the break in the standard-deviation plot, where data from two separate test runs are plotted. Nevertheless, the only effect of this lower than expected performance was to shorten the star update interval.

### Software

The software design is, in general, characterized by achievement of required system performance with a minimum of equation complexity. A functional block diagram of the software algorithms is shown in Fig. 3. Inertial attitude is derived by integration of the gyros pulse count outputs. A Kalman filter is employed for periodic star tracker updates to bound the gyro error. A star catalog provides star position coordinates.

The attitude algorithm uses Euler symmetric parameters to propagate the attitude through numerical integration. A closed form solution was used to inhibit the truncation errors inherent in a power series characterization. The Kalman filter state vector was comprised of six elements: three attitude variables and three gyro drift-rate biases. The extended Kalman filter formulation was utilized where linearization is performed about the previous attitude estimate. Values for the state error covariance matrix were selected based upon the measured gyro performance data. Elements of the measurement noise-covariance matrix were based on measured star-tracker noise.

**Table 1 Strapdown star tracker characteristics**

| | |
|---|---|
| Field of view | $1 \times 1$ deg |
| Sensitivity | 10 $M_v$ GO(6000 K) |
| Photodetector | |
| Type | ITT F4012 |
| Usable photocathode area | 0.5 in. dia |
| Aperture diameter | 0.010 in. |
| Optics | |
| Type | Cassegrain |
| Focal length | 20 in. |
| Aperture | 60 cm$^2$ |
| Instantaneous field of view | 103 arc-s |
| Electronics | |
| Position output | 12 bit serial word |
| Magnitude output | 10 bit serial word |
| Update time | 0.1 s |
| Functional performance | |
| Maximum acquisition time | 12.8 s |
| Maximum track rate | 0.06 deg/s |
| Accuracy (with FOV and temp. comp.) | |
| Line of sight to EO axes | |
| Noise ($1\sigma$) (single sample) | 3.0 arc-s (8 $M_v$) |
| Fixed ($1\sigma$) | 2.0 arc-s |
| EO axes to optical reference bias ($3\sigma$) | 2.4 arc-s |
| Size | $5 \times 5 \times 22$ in. |
| Weight | 11 lb |
| Power | 4.6 W |

## III. Test Configuration

A number of pragmatic decisions had to be made involving the design of the test configuration. The most important concerned the fact that only one strapdown star tracker was available within the resources of the program. Since practically no geometric leverage exists about the boresight of a $1 \times 1$ deg field of view the system performance goal could be achieved only about the two axes normal to the boresight; in essence, a two-axis test was conducted for the strapdown system.

Another decision involved the technical impossibilty (within the program scope) to simulate bright-object interference. In view of this, the assumed orientations of the tracker fields of view in orbit were picked to make sensor errors as nearly as possible one-to-one with system errors.

**Table 2 Gimbaled star tracker characteristics**

| Design characteristics | |
|---|---|
| Field of view | $0.5 \times 0.5$ deg |
| Gimbal freedom | $\pm 45$ deg |
| Sensitivity | $+3.5\ M_v$ |
| Bandwidth | 25 Hz |
| Optics | |
| Focal length | 84 cm |
| Aperture | 54 cm$^2$ |
| IFOV | 84 arc-s |
| Detector | F4012 RP |
| Minimum sun angle | 45 deg |
| Size (with shade) | $11.8 \times 20.0 \times 6.4$ in. |
| Weight | 24 lb |
| Power | 9 W |

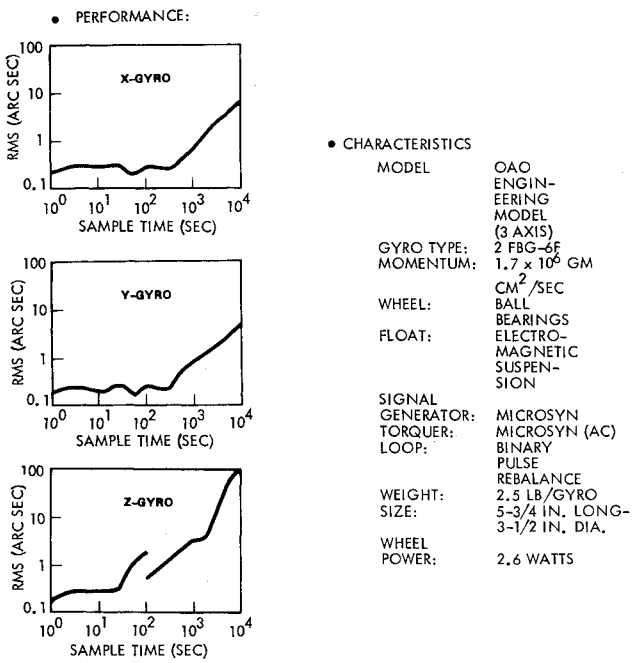


**Fig. 2 Inertial reference unit characteristics.**

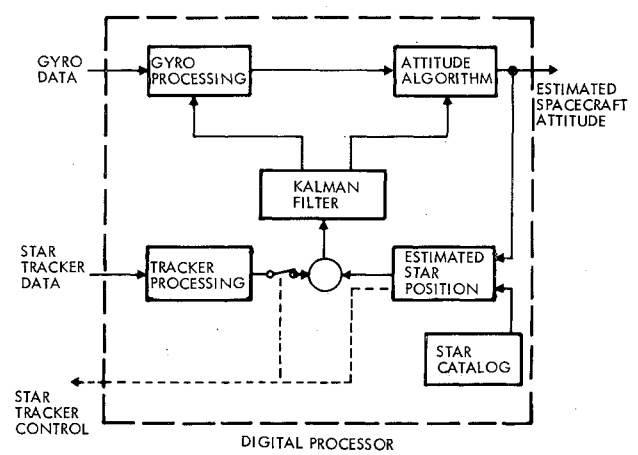


**Fig. 3 Software algorithms.**

### Simulated Orbit Configuration

With the foregoing considerations in mind, the simulated orbit configurations that evolved are shown in Fig. 4. The strapdown system is a two-axis system consisting of one narrow field of view tracker and two gyros whose input axes are orthogonal to the field boresight and to each other. The boresight axis points to the celestial equator for maximum star availability.

The gimbal system is a three-axis system since the 90 deg sweep of the tracker boresight axis does give adequate geometric leverage for three-axis tracker information. This system is also supplemented by three orthogonal gyros. The center of the sweep is also pointed to the celestial equator for maximum star availability.

The driving function for star update frequency is the random drift of the gyros. For the particular gyros used, a nominal update period of 20 min was chosen. This is equivalent to acquiring a star every 5 deg of right ascension in geosynchronous orbit. With the strapdown tracker able to track 8 $M_v$ stars, and the gimbaled tracker 3.5 $M_v$ stars, a 20-min period gives a 0.9736 or greater probability of at least one star occurring in the field of view of either tracker.

Although the system tests were performed with stars occurring every 20 min, in the evaluation of the test data a parametric analysis of the effect of update period was obtained by skipping updates. In this manner, 40- and 60-min update periods were also obtained.

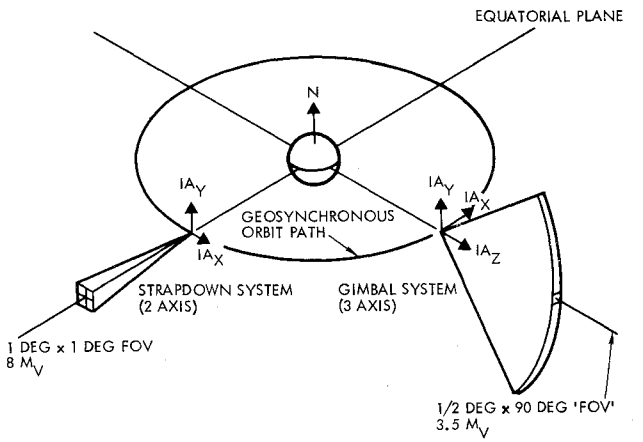


**Fig. 4 Simulated orbit configurations.**

Three different star declinations were used for both systems. For the strapdown system, the purpose of multiple declinations was to exercise the accuracy of the tracker at more than one place in the field of view. For the gimbal system, the motivation was to obtain three-axis information as well as to exercise the accuracy of the gimbal readout.

### Laboratory Test Configurations

The key feature of the laboratory test configurations for both system tests was that a ground-fixed test was implemented. The earth rotation was used directly to simulate the inertial motion of an earth-pointed geosynchronous satellite by fixing the PADS sensors relative to the laboratory floor, which itself is a seismic pad isolated from building vibrations. The stellar optical stimuli were simulated by sweeping collimated star beams past the stationary PADS star tracker.

The ground-fixed test provided two advantages over the more conventional approach of rotating the PADS on a rate table in the center of a room, and placing multiple star sources around the room which point at the rotating PADS. The first is that the ground-fixed approach is compatible with the parallel beam star stimulus technique described later. This technique is essential to providing instrumented knowledge of star location to 1-arc-s accuracy. The second advantage is that the artificial vector subtraction of earth rate from the gyro outputs is not necessary in the ground-fixed approach. This subtraction can cause additional system errors, especially in this case where the subtracted vector has the same magnitude as the gyro output vector.

In aligning and testing the PADS system, its reference axes are identical to the laboratory axes. Both are physically defined by optical surfaces on the star trackers. The strapdown star tracker used the normals to two faces of an optical cube to define its axes. The gimbal star tracker used an orthogonal set of axes whose orientation was defined relative to three mirror surfaces on the tracker base.

Star catalog information is obtained by the measurement with laboratory instrumentation of the star orientation relative to laboratory axes. It is essential that the catalog information be accurate since an error here propagates directly into an error in the measured accuracy of the PADS.

### Parallel Beam Star Stimulus Technique

The key test configuration requirement is to know the instantaneous orientation of the star line of sight relative to the laboratory axes. Since the PADS performance requirement is 3.6 arc-s, knowledge of the orientation of the rotating, collimated star beam must be significantly better than this value. By using a parallel beam star stimulus technique, an accuracy of 1 arc-s appeared achievable.

The parallel beam technique is best illustrated by the top view of the strapdown system test configuration shown in Fig. 5. Functionally, the performance of a star transit (defined as a sweep of a star through the field of view of the tracker) is straightforward. The collimated star beam from the star source is reflected off the rotating mirror mounted on top of the air bearing table. The table is turned at half earth rate so that the reflected star beam sweeps past the star tracker at earth rate. To measure where the star beam is relative to the PADS axes, i.e., the optical cube on the right side of the star tracker, the collimated beam from an automatic autocollimator is transmitted parallel to the star beam. The normal to the front face of the cube is the defined boresight axis of the tracker. When the star beam (center star) is coincident with the boresight axis, the autocollimator beam will be normal to the front face, and the horizontal and vertical output of the two-axis autocollimator will be zero.

The automatic autocollimator is used for a static indication of the star orientation in a small region around the boresight axis. For a wider range (1 deg) and higher dynamic response (1 arc-s per rad/s), the air bearing table readout is used. The zero reference for the readout is obtained by making a static table reading at the boresight position indicated by the automatic autocollimator.

So far this discussion has been limited to measuring the location of the center star relative to the PADS axes. By independently measuring the relative locations of the other two stars to the center star, their locations relative to the PADS axes can also be determined by the parallel beam technique. The independent measurements were made with a theodolite. The gravity vector was used as a reference for rotations about the boresight axis.

The key to the success of the parallel beam method is the ability to recalibrate as frequently as necessary the parallelism between the collimated center star and autocollimator beam. This is facilitated by use of the theodolite and double-sided mirror shown in Fig. 5. The double-sided mirror is positioned half way in front of the aperture of the theodolite. The backside mirror is positioned perpendicular to the theodolite boresight by using the autocollimator feature of the theodolite. Since the frontside mirror is parallel to the backside mirror, the normal to the frontside is then parallel to the telescope boresight of the theodolite. Both can now be used to calibrate the parallelism between the two collimated beams. The air bearing table is rotated until the star beam is along the boresight of the theodolite. When this condition exists, the automatic autocollimator will adjust its beam normal to the frontside mirror. Any deviations from zero of the autocollimator horizontal and vertical outputs represent its null bias errors. The utility of this recalibration method is that it can be performed at any time during a test period.

The major advantage of the parallel beam technique is that it eliminates the temporal attitude drifts that so often plague achievement of arc-second accuracy. Since the parallel beams are used, the technique is insensitive, for example, to a motion of the star tracker during warmup, to long-term settling of the granite table, or to disturbances of the star source/autocollimator assembly. Although it is sensitive to autocollimator null drifts, even this error source is neutralized by the ability to recalibrate as frequently as necessary.

## IV. Test Facility

The test facility consists of four areas: 1) a laboratory, 2) a control platform, 3) a computer area, and 4) a work area. The laboratory is a darkroom positioned on a seismic pad isolated from building vibrations. The laboratory has its own air conditioning system that controls the air temperature to 0.6°C. In general, all heat-generating equipment was located outside the laboratory to minimize thermal gradients. Equipment installation settling times of 60 days or more were allowed for the star source, the granite tables, and the air bearing table.

All electronic equipment necessary to monitor and control the system tests was located on the control platform. The computer area contained a CDC 1700 digital computer and two control terminals. Although the computer implemented the control of various equipment during a test run, control of the computer itself was exercised from switches on the control platform.

The facility data handling and display configuration is illustrated in Fig. 6. Data were generated during the system tests from two sources: the PADS sensor and the laboratory instrumentation. The data served two purposes: to provide the basis for evaluation of the PADS under test, and to provide real-time diagnostic data to indicate the validity of the test.

## V. Performance Evaluation Technique

The performance evaluation of the PADS test data was performed offline on a CDC 6500 digital computer whose input consisted of the magnetic tape sensor data from the laboratory computer and certain initialization and control parameters. Separate programs, representing Kalman-filter

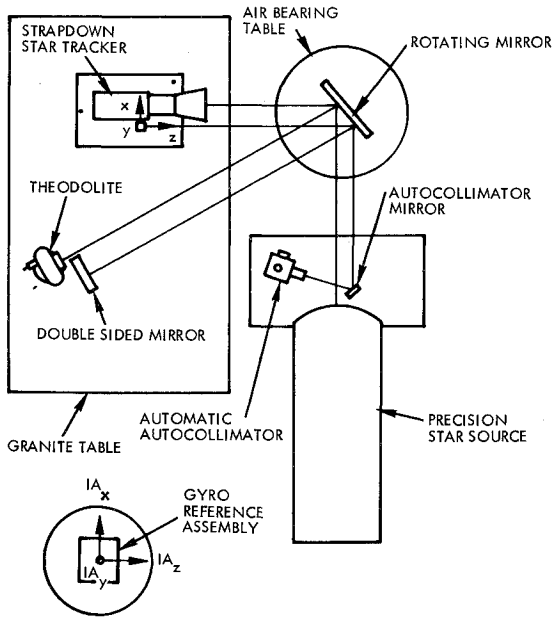


Fig. 5 Example of parallel-beam star stimulus technique.

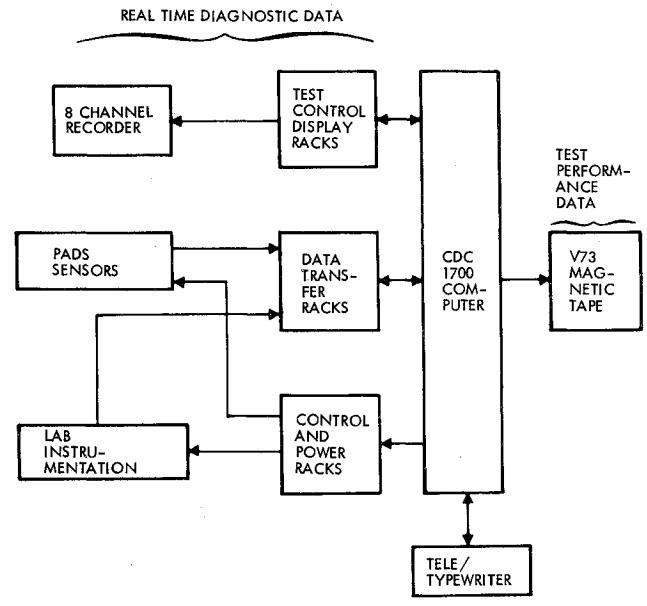


Fig. 6 Test facility data handling and display.

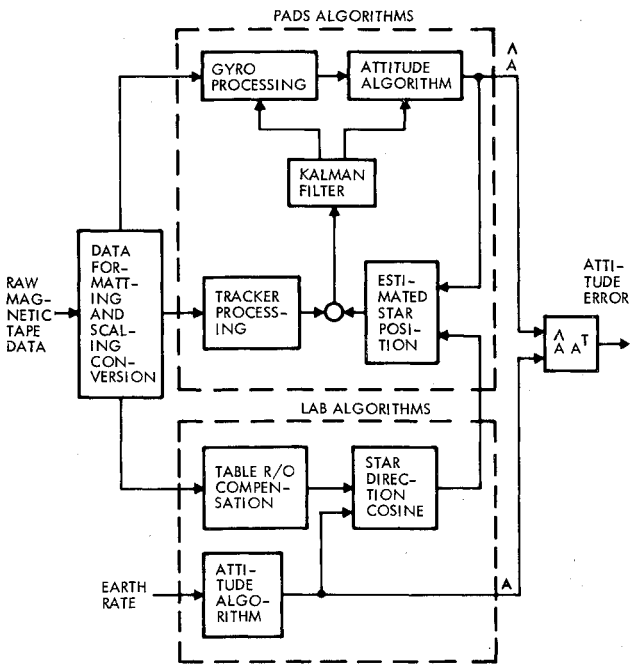


**Fig. 7 Offline data evaluation.**

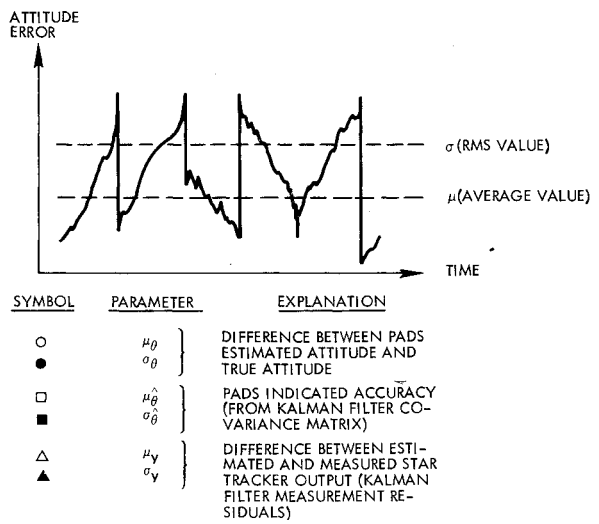


**Fig. 8 Steady-state attitude error performance measures.**

estimators, were developed for the strapdown and gimbal tests. A functional block diagram applicable to either computer program is shown in Fig. 7. Note that the laboratory algorithms indicated in the figure are required only to generate attitude and star source data and are thus not part of an operational PADS system.

The output of these attitude estimators is defined by establishing an inertial set of coordinate axes indicative of the spacecraft (or PADS) axes orientation. The chosen inertial set was taken to represent the coordinate axes of the optical cube at the start of the test, time $t_0$. Subsequent orientation of this cube is then described by a direction cosine matrix, $A(t)$, where $A(t_0)$ is the identity matrix. If $u_s$ is the unit vector of a simulated star in laboratory coordinates, then $A^T(t)u_s$ represents the inertial description of this star. It is important to note that $A(t)$ also describes the *actual* attitude of the PADS system due to the alignment procedure previously described, and that the attitude estimates provided by the Kalman filter computer programs must closely reflect $A(t)$ if they are to be effective.

The Kalman filter attitude estimator is, of course, not privy to information regarding the alignment of PADS in the laboratory, but is permitted to derive this information only after processing of the star tracker and gyro sensor data. The estimate of the PADS attitude will thus be denoted by $\hat{A}(t)$, with the initial estimate $\hat{A}(t_0)$ reflecting a 100-arc-s attitude error in each of the coordinate axes. Also, comparable uncertainties are assumed in the filter's error covariance matrix. The accuracy of the attitude estimate is then given by the components of $A(t)-\hat{A}(t)\approx\hat{A}(t)A^T(t)$ at any time $t$. Test results illustrating the filter's effectiveness as a function of time are presented in the next section.

Two figures of merit were defined for the strapdown system steady-state performance. Letting $\theta_1$ and $\theta_2$ represent attitude estimation errors in the components normal to the boresight axis, define

$$\theta=\sqrt{\theta_1^2+\theta_2^2} \tag{1}$$

The figures of merit are then

$$\mu_\theta=\frac{1}{t_f-t_s}\int_{t_s}^{t_f}\theta(t)\,dt \tag{2}$$

$$\sigma_\theta=\left\{\frac{1}{t_f-t_s}\int_{t_s}^{t_f}\theta^2(t)\,dt\right\}^{1/2} \tag{3}$$

where $t_f$ is the final test time (4 h) and $t_s$ is a time at which transient effects of the filter's convergence can be ignored. Similar figures of merit were adopted for the gimbaled PADS system except that all three attitude components were included in the definition of $\theta$.

While $\mu_\theta$ and $\sigma_\theta$ demonstrate the filter's effectiveness, its integrity is measured by how well the uncertainties reflected by its error covariance matrix compare to its actual estimation errors. In analogy to Eqs. (2) and (3), $\mu_{\hat{\theta}}$ and $\sigma_{\hat{\theta}}$ were formed, where $\hat{\theta}(t)$ was derived from the covariance matrix. Close correspondence of $\mu_{\hat{\theta}}$ to $\mu_\theta$ and $\sigma_{\hat{\theta}}$ to $\sigma_\theta$ is clearly desirable.

Yet a third measurable criterion exists, namely the degree to which the Kalman filter's predicted star-tracker measurements subsequently reflect the actual data. Using a similar calculation, $\mu_y$ and $\sigma_y$ were formed, which again should be consistent with their attitude counterparts. Figure 8 summarizes these concepts, and defines symbols that will subsequently be used in presenting test results.

## VI. Test Results

Both the strapdown and gimbal system tests were based on the following scenario. A PADS system is on board a three-axis-stabilized, earth-pointed satellite in geosynchronous orbit. Also on board is an experiment, for example, a telescope, that requires precise information as to the inertial attitude of its sensitive axis or axes. The PADS is used to provide this information. A calibration of the PADS star-tracker boresight axis relative to the experiment axes is performed once every 10 days. Following the calibration, the experiment may require the PADS attitude information for any length of time, for any number of times, during the next 10 days.

The strapdown and gimbal system tests were performed during separate 10 day test periods. By way of configuring a practical laboratory test, four test runs, nearly evenly spaced in time, were conducted during each 10-day period. Each run was approximately 4 h in duration. During each run, a star update was made every 20 min. For the strapdown test, 8 $M_v$ stars were used at three different declinations: $-0.1$, 0.0, and 0.3 deg. For the gimbal system test, 3.5 $M_v$ stars were used at three declinations: $-23.0$, $-4.0$, and 14.9 deg.

### Convergence Error

Typical attitude error convergence plots for the strapdown and gimbal systems are shown in Figs. 9 and 10, respectively. Initial attitude errors of 100 arc-s in each axis were used. The

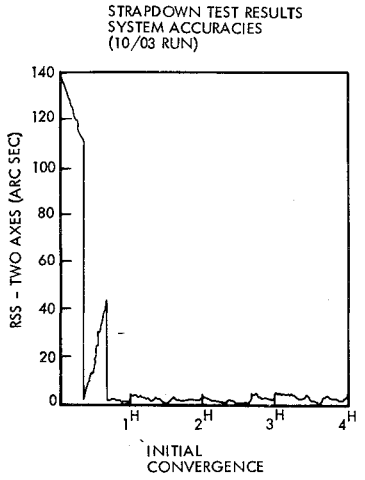


Fig. 9 Example of strapdown system attitude-error convergence.

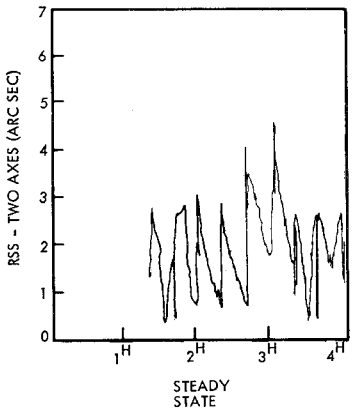


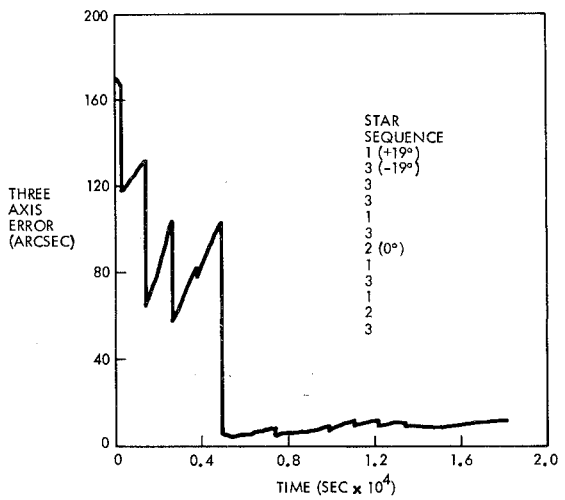


Fig. 10 Example of gimbal-system attitude-error convergence.

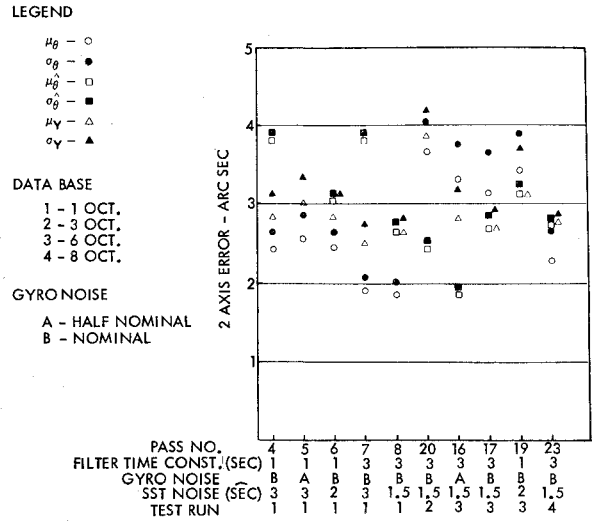


Fig. 11 Strapdown-system parametric results.

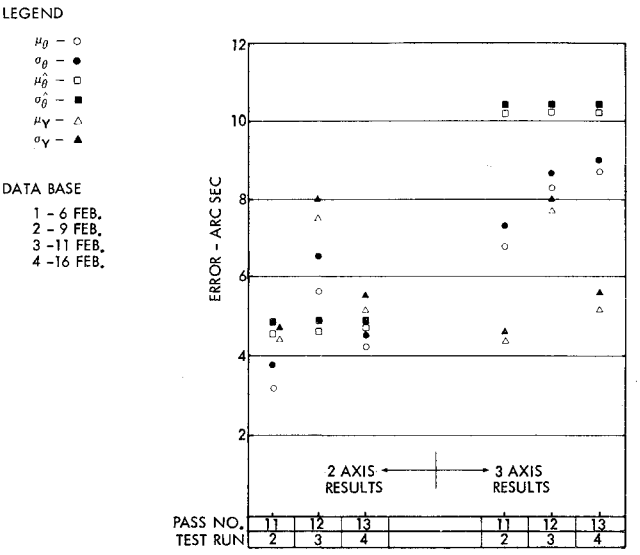


Fig. 12 Gimbal-system parametric results.

two-axis error of the strapdown system drops immediately to the accuracy of the star tracker after the first update. However, two updates are necessary before the Kalman filter can estimate the gyro drift rate. Thereafter, typical steady-state performance is indicated. The situation is more complicated in the case of the gimbal system since the filter is dependent not only on the number of updates but also on the separation angles between stars. The star declinations used in Fig. 10 started out as 14.9, −23.0, −23.0, −23.0, 14.9 deg, and so forth. The first update drops the error down close to the single-axis uncertainty of 100 arc-s. However, even though the next three updates are separated from the first by 38 deg, the filter is unable to resolve both the three-axis attitude error and the gyro drift uncertainties given only one change in declination angle. The situation is rectified when the fifth update gives the second change in declination angle. Thereafter, the filter has essentially reached steady state in both its attitude and drift-rate steady-state estimates.

### Steady-State Error

For each system test, the time-tagged data for the four runs were processed by the software algorithms to predict both PADS attitude and gyro drift rate. In addition to these data, the algorithms required inputs dealing primarily with a priori statistical quantities used in the Kalman filter. This information describes initial uncertainties in attitude and gyro drift rates, as well as the star-tracker and gyro-noise parameters. In general, the performance of the filter is dependent upon the closeness of the correlation between the statistical quantities and the actual hardware.

For a parametric evaluation of the effectiveness of the filter, several computer passes were made in which the data from the test runs were processed by the algorithms, which in turn had been initialized with different values for the sensor parameters. Figures 11 and 12 are plots of the results from some of these passes for the strapdown and gimbal tests, respectively. For example, pass no. 4 in Fig. 11 used the test data obtained on Oct. 1, assumed nominal gyro noise parameters, a star-tracker noise of 3 arc-s ($1\sigma$), and passed the

tracker output through a 1 s first-order lag filter prior to its use by the filter. Fairly close agreement of comparable figures of merit for all but a couple of passes was obtained.

For the gimbal test (Fig. 12), a distinction is made between two- and three-axis results. The two-axis result does not include the error about the axis which is nearly coincident with the middle star. It is about this axis that the limited separation between stars (19 deg) contributed an effect. Thus, for comparative purposes the two-axis gimbal result can be compared to the two-axis strapdown result.

Again, for a parametric evaluation of the effect of star update interval on total accuracy, a number of computer passes were made in which only every other star update was used. In this manner $\sigma_\theta$ was obtained for 20-, 40-, and 60-min update periods. The results for the strapdown and gimbal tests are shown in Tables 3 and 4, respectively.

The PADS design goal was 3.6 arc-s ($1\sigma$) per axis for 20-min star updates. The measured errors of 2.3 and 3.6 arc-s for the strapdown and gimbal systems, respectively, met this goal. In fact since the values in the two tables reflect both PADS and laboratory instrumentation errors, the systems are probably more accurate than these values indicate.

#### Comparative Performance

In a comparative sense, the performance of the strapdown system convincingly exceeded that of the gimbal system. Subsequent analysis of the test data indicated that some of the difference in performance could be attributed to drifts in the electro-optical boresight of the gimbaled star sensor. Also, alignment complexities that were encountered during the setup of the gimbal test, specifically those that involved the gimbaled star tracker, were more numerous than those of a comparable strapdown system with two star trackers. These complexities arise primarily from the inability to directly identify the gimbal axis with an optical flat in the presence of a 1$g$ field. In another aspect, the hardware-connected difficulties encountered during the test of the gimbaled star tracker provided a reminder of the complexity of that unit relative to the strapdown star tracker.

On the other hand, the comparison in accuracy made here was for a specific application, namely that of a three-axis-stabilized, earth-pointed satellite in geosynchronous orbit. In other applications, involving less predictable spacecraft rates, the more versatile aspects of the gimbal PADS may well outweigh the accuracy criteria.

#### Laboratory Instrumentation Errors

The results obtained in the area of minimizing the laboratory instrumentation errors were very satisfactory, primarily due to the parallel beam star stimulus technique. Analytically predicted instrumentation errors of 0.9 and 1.6 arc-s for the strapdown and gimbal tests, respectively, most probably were achieved in view of the overall test results. The minimization of these errors gave the advantage of presenting PADS attitude errors as measured, without qualifications.

While the parallel beam star stimulus technique did minimize the instrumentation errors, it also made clear that the limit in test accuracy for star trackers and stellar attitude determination systems was reached using commerically available instrumentation. The fundamental limitation was the theodolite: its repeatability and its circle accuracy. Obtaining accuracies better than 0.5 arc s, even with the best instrument available, is doubtful.[9,10] Another limitation is the accuracy of mirror surfaces, their flatness, and their parallelism and perpendicularity to each other. Procurement of such mirrors with specifications equivalent to 1 arc-s is not only costly but often beyond the capabilities of most optical suppliers. Stability and collimation accuracy of star sources are other limitations. Thermal gradients, material creep, and long-term deformations make arc-second accuracies difficult to achieve.

**Table 3 Strapdown system accuracy**

| | Test results | | |
|---|---|---|---|
| Test run | 20 min-updates | 40-min updates | 60-min updates |
| 1 | 2.0 | 2.3 | 3.3 |
| 2 | 4.0 | 7.1 | 13.5 |
| 3 | 3.7 | 5.7 | 8.3 |
| 4 | 2.7 | 3.6 | 5.8 |
| rms (2-axis) | 3.2 | 5.0 | 8.6 |
| rms (1-axis) | 2.3 arc-s | 3.6 arc-s | 6.1 arc-s |

**Table 4 Gimbal system accuracy**

| PADS rms error for two-axis results | | | |
|---|---|---|---|
| Test run | 20-min updates | 40-min updates | 60-min updates |
| 1 | – | – | – |
| 2 | 3.8 | 3.2 | – |
| 3 | 6.6 | 7.1 | – |
| 4 | 4.5 | 5.3 | 6.5 |
| rms (2-axis) | 5.1 | 5.4 | 6.5 |
| rms (1-axis) | 3.6 arc-s | 3.8 arc-s | 4.6 arc-s |
| **PADS rms error for three-axis results** | | | |
| Test run | 20-min updates | 40-min updates | 60-min updates |
| 1 | – | – | – |
| 2 | 7.3 | 4.6 | – |
| 3 | 8.6 | 23.3 | – |
| 4 | 8.9 | 6.6 | 15.0 |
| rms (3-axis) | 8.3 | 14.2 | 15.0 |
| rms (1-axis) | 4.8 arc-s | 8.2 arc-s | 8.7 arc-s |

It seems clear that if star trackers or attitude determination systems with sub-arc-second accuracies are developed, a significant increase in the cost of testing such units or systems will be experienced. A large part of the test cost will be the development and certification of the precision test instrumentation required.

## VII. Conclusions

The laboratory tests demonstrated that either the strapdown or gimbal PADS, under laboratory-controlled temperature and vibration environments, will meet the design goal of 3.6 arc-s ($1\sigma$) per axis.

The attitude error convergence characteristics for both systems indicate that the limiting factor for the 20-min update intervals was the star tracker error. Independent evaluations of the tracker noise and bias errors led to the conclusion that the software algorithms, and the Kalman filter specifically, did not add significantly to the total error.

## Acknowledgment

The test program described herein was accomplished under the Application of Precision Attitude Determination Systems Program (NAS 1-12894) funded by NASA Langley Research Center. Appreciation is extended to D. Hinton of NASA-Langley for his patience and guidance throughout the program, and to H. Hoffman of NASA Goddard Space Flight Center for providing the OAO gyro assembly. Special thanks are extended to R. Carson of Charles Stark Draper Laboratory for his efforts in integrating the gyros to the PADS system.

## References

[1] Frew, A.M., Kirby, D.K., Wheeler, P.C., and Huber, T.C., "An Integrated System for Precision Attitude Determination and Control," AIAA Paper 71-962, Hempstead, N.Y., Aug. 1971.

[2] Farrenkopf, R.L., and Iwens, R.P., "Performance Evaluation of a Precision Attitude Determination System (PADS)," AIAA Paper 71-964, Hempstead, N.Y., Aug. 1971.

[3] Gates, R.F., and McAloon, K.J., "A Precision Star Tracker Utilizing Advanced Techniques and Materials," AIAA Paper 76-113, Washington, D.C., Jan. 1976.

[4] Gates, R.F., Eisenhut, D., Zaremba, G., and Kalley, J., "Ultra High Accuracy Gimbaled Star Tracker," AIAA Paper 71-963, Hempstead, N.Y., Aug. 1971.

[5] Davis, W.R., et al, "Precision Earth Pointing System (PEPSY) Phase 1B Final Report," SAMSO TR 70-433.

[6] Toda, N.V., Heiss, J.L., and Schlee, F.H., "SPARS: The System, Algorithms, and Test Results," Symposium on Spacecraft Attitude Determination, The Aerospace Corporation, Oct. 1969.

[7] Schlee, F.H. and Neilsen, G., "Laboratory Checkout and Testing of an Advanced Stellar Inertial Attitude Reference System," Symposium on Spacecraft Attitude Determination, The Aerospace Corporation, Oct. 1969.

[8] Harris, R.A., "In-Orbit Performance of the OAO Inertial Reference Unit," *Journal of the Institute of Navigation,* Vol. 21, Winter 1974-75.

[9] Popelka, M.F., and Ferren, F.R., "Astro-Azimuth Comparative Studies with Wild T3, Wild T4, and Kern DKM3 Theodolites," AIAA Paper 72-842, Stanford, Calif., Aug. 1972.

[10] Fondelli, M., "Examination of the Precision of Kern DKM3 Theodolites," Military Geographic Institute, Florence, Italy, 1957.